On the distribution of galaxy ellipticity in clusters

F. D'Eugenio,[1,2,3]★ R. C. W. Houghton,[1] R. L. Davies[1] and E. Dalla Bontà[3,4]

[1]*Sub-department of Astrophysics, Department of Physics, University of Oxford, Denys Wilkinson Building, Keble Road, Oxford OX1 3RH, UK*
[2]*Research School of Astronomy and Astrophysics, Australian National University, Canberra, ACT 2611, Australia*
[3]*ARC Centre of Excellence for All-Sky Astrophysics (CAASTRO)*
[4]*Dipartimento di Fisica e Astronomia "G. Galilei", Università degli Studi di Padova, Vicolo dell'Osservatorio 3, I-35122 Padova, Italy*
[5]*INAF Osservatorio Astronomico di Padova, Vicolo dell'Osservatorio 5, I-35122, Padova, Italy*

ABSTRACT

We study the distribution of projected ellipticity $n(\epsilon)$ for galaxies in a sample of 20 rich (Richness ≥ 2) nearby ($z < 0.1$) clusters of galaxies. We find no evidence of differences in $n(\epsilon)$, although the nearest cluster in the sample (the Coma Cluster) is the largest outlier (P(same) < 0.05). We then study $n(\epsilon)$ within the clusters, and find that ϵ increases with projected cluster-centric radius R (hereafter the ϵ-R relation). This trend is preserved at fixed magnitude, showing that this relation exists over and above the trend of more luminous galaxies to be both rounder and more common in the centres of clusters. The ϵ-R relation is particularly strong in the subsample of intrinsically flattened galaxies ($\epsilon > 0.4$), therefore it is not a consequence of the increasing fraction of round slow rotator galaxies near cluster centers. Furthermore, the ϵ-R relation persists for just smooth flattened galaxies and for galaxies with de Vaucouleurs-like light profiles, suggesting that the variation of the spiral fraction with radius is not the underlying cause of the trend. We interpret our findings in light of the classification of early type galaxies (ETGs) as fast and slow rotators. We conclude that the observed trend of decreasing ϵ towards the centres of clusters is evidence for physical effects in clusters causing fast rotator ETGs to have a lower average intrinsic ellipticity near the centres of rich clusters.

Key words: galaxies: clusters: general – galaxies: elliptical and lenticular, cD – galaxies: photometry.

1 INTRODUCTION

Early-type galaxies (ETGs) account for half of the stellar mass in the local Universe (Renzini 2006). They are traditionally divided in two subclasses: elliptical (E) and lenticular (S0) galaxies. To first order, Es have smooth, single-component light profiles, while S0s present both a central bulge and an extended stellar disc. ETGs are more common in clusters of galaxies, and the morphology–density relation (T–Σ; Dressler 1980) illustrates the effect of the local environment on the formation and evolution of these galaxies [Whitmore, Gilmore & Jones (1993) argue however that the morphology correlates better with the cluster-centric radius]. Dressler et al. (1997) used *Hubble Space Telescope* (*HST*) photometry to show that cluster Es are already in place at redshifts $z \approx 0.5$, while the fraction of S0s is lower than in the local Universe. Therefore, Es form earlier than S0s, which arise from infalling late-type galaxies

mostly between $z \approx 0.5$ and $z = 0$ (e.g. Vulcani et al. 2011, but see Holden et al. 2009 for a different view).

The division between Es and S0s presents however a number of problems. Observationally, it is difficult to distinguish Es from close-to-face-on S0s, and morphological catalogues might be biased in this sense (van den Bergh 1990). Galaxies classified as Es are often found to contain disc components (Kormendy & Djorgovski 1989). Rix & White (1990) further demonstrated how discs can go undetected even in local galaxies. All but the brightest Es and S0s in the Coma Cluster form a family with continuous bulge-to-disc light ratios (B/D; Jørgensen & Franx 1994). More recently, the SAURON survey (de Zeeuw et al. 2002) used integral field spectroscopy (IFS) to investigate the stellar kinematics of ETGs. They identified two dynamical classes within ETGs: fast rotators (FRs) and slow rotators (SRs). The former exhibit large-scale rotation patterns typical of a disc origin, while the latter have little to no rotation (Cappellari et al. 2007; Emsellem et al. 2007). Importantly, both SRs and FRs are found amongst both Es and S0s. The volume-limited ATLAS[3D] survey (Cappellari et al. 2011a) determined that 66 per cent of the local Es are FRs (Emsellem et al. 2011), and a new classification

★ E-mail: francesco.deugenio@anu.edu.au

paradigm has been invoked (Cappellari et al. 2011b; Kormendy & Bender 2012).

In particular, FR ETGs form a sequence of increasing disc fraction, parallel to that of spiral galaxies (the comb diagram; Cappellari et al. 2011b). The emerging picture is that – kinematically – FR ETGs are much more similar to spiral galaxies than they are to SR ETGs. Unfortunately, IFS observations, which are necessary to tell apart FRs from SRs, are time consuming when compared to photometry. Even the largest upcoming IFS surveys (SAMI, Croom et al. 2012, MaNGA, Bundy et al. 2015) have sample sizes which are several orders of magnitude smaller than current state-of-the-art photometric surveys, like SDSS. Here we investigate whether we can take advantage of currently available photometric samples to investigate the properties of ETGs in the framework of the FR/SR classification.

Using photometry alone, ETGs can be characterized by their projected ellipticity $\epsilon \equiv 1 - q$, where q is the apparent axial ratio. The observed value of ϵ depends both on the distribution of the orbits (which determines the *intrinsic* ellipticity) and on the inclination of the galaxy on the plane of the sky. In general, it is not possible to infer the 3D structure of an individual galaxy from its photometry alone, but we can study intrinsic shapes statistically (Sandage, Freeman & Stokes 1970; Lambas, Maddox & Loveday 1992). These studies showed that the distribution of ellipticity $n(\epsilon)$ for Es and S0s is different, with Es on average rounder than S0s. More recently, Weijmans et al. (2014) used the ATLAS[3D] sample of ETGs to show that the intrinsic shape of FRs (both Es and S0s) is consistent with that of spiral galaxies, with an average axial ratio $q = 0.25 \pm 0.01$. This reinforces the view that FR ETGs and spiral galaxies form a family of intrinsically flat stellar systems.

Kuehn & Ryden (2005, hereafter KR05) studied the relation between q and the local environment using a magnitude limited sample ($r < 17.77$ mag). They found that galaxies with different magnitude and light profile exhibit different trends of ϵ with the local number density of galaxies. Galaxies characterized by a de Vaucouleurs light profile (de Vaucouleurs 1948) are rounder in denser environments, regardless of their luminosity. Galaxies with exponential profiles show two opposite tendencies, based on their absolute magnitude. Galaxies fainter than $M_r = -20$ mag are rounder in denser environments, while more luminous galaxies tend to become flatter at higher density. These results suggest that the environment can affect the shape of galaxies. Intriguingly, the trend observed by KR05 is strongest when the density is measured inside an aperture with diameter $2\,h^{-1}$Mpc, which roughly corresponds to the size of a cluster of galaxies.

Here we propose to investigate $n(\epsilon)$ for cluster galaxies, in the framework of the SR/FR paradigm. In particular, since there are no SRs with $\epsilon \geq 0.4$ (Emsellem et al. 2011), we can remove them from any photometric sample. In the next section, we introduce our sample of local cluster galaxies, and proceed to show the results of the analysis. We then discuss possible sources of bias, and whether the observed relation is a consequence of previously known trends. We conclude with a summary of our results.

2 DATA AND SAMPLE

To assess the effect of the environment on the apparent ellipticity of galaxies, we study a sample of rich nearby clusters of galaxies with SDSS DR10 data (Ahn et al. 2014). At low redshift ($z \lesssim 0.04$), the most complete catalogue of clusters is that of Abell, Corwin & Olowin (1989), from which

(i) we discarded all the clusters with $z > 0.1$, or with no redshift measurement available;

(ii) we discarded all clusters with richness $\mathcal{R} < 2$ because we expect any signature of the cluster environment to be strongest in rich systems.

This left 20 clusters (see Table 1). For each of them, we retrieved SDSS photometry as follows.

(i) We determined the centre of the cluster as the coordinates of the brightest galaxy. When the second brightest galaxy falls within 0.5 mag from the brightest, we used the mid-point between the brightest and second brightest as the centre of the cluster (e.g. Abell 1656, Abell 1367).

(ii) We queried the table 'Galaxy' from the SDSS DR10 data base, retrieving all the galaxies within a projected radius of 1.5 Mpc from the cluster centre. The angular distance was derived by assuming Planck Cosmology ($\Omega_m = 0.32$, $\Omega_\Lambda = 0.68$, $h_0 = 0.67$; Ade et al. 2014). We assume zero peculiar velocity for all the clusters.

(iii) We removed all galaxies with a radius *deVRad*[1] ≤ 0.4 arcsec (corresponding to 0.5 kpc at $z = 0.1$). This constraint filters out artefacts and measurements with bad photometry, which are otherwise still present in the table Galaxy.

(iv) We further removed objects that are classified as stars in the g' and i' bands (SDSS uses only the r' band for this classification). This condition filters out 31 objects. Objects with negative or zero errors in the photometry were also eliminated (21 objects in total).

(v) We applied a cut in absolute magnitude at $M_r = -18.0$ mag. This is well above the r'-band completeness limit of SDSS at redshift $z = 0.1$ (the maximum distance modulus for our sample of clusters is ≈ 38 mag). A more generous magnitude cut increases the scatter in the red sequence (RS), which is undesirable. We do not apply a *k*-correction, but this does not affect our results.

For each galaxy, we retrieved the SDSS r'-band *ModelMag* as a measure of magnitude and $g' - r'$ colours using SDSS *AperMag*.

Ancillary data consist of SDSS DR10 spectroscopic redshifts for a sample of galaxies in the cluster Abell 1656 (the Coma Cluster), and of Galaxy Zoo 2 (GZ2; Willett et al. 2013) morphological classifications, when available.

2.1 Projected ellipticity

SDSS offers two different measures of ellipticity. The model ellipticity is defined as $1 - b/a$, where b/a is the apparent axial ratio of the r'-band best-fitting model (i.e. $b/a \equiv deVAB\_r$ if $fracDeV\_r \geq 0.5$ and $b/a \equiv expAB\_r$ if $fracDeV\_r < 0.5$). The SDSS pipeline automatically corrects the model axial ratio for the effect of the point spread function (PSF; see Section 4.1 for a discussion).

An alternative measure of the ellipticity is to use the adaptive second-order moments of the surface brightness *I*. This method uses a Gaussian weight function adaptively matched to the size and shape of the galaxy being measured (Bernstein & Jarvis 2002; Hirata & Seljak 2003).

Comparing the model ellipticity to the moments ellipticity in the r' band, we find that in general the former is larger. The best linear fit yields $\epsilon_{model} = (1.039 \pm 0.004)\epsilon_{moments} + (0.025 \pm 0.001)$ (Fig. 1). As in general ϵ increases with radius within galaxies, ϵ_{model} is better suited for the outer region of galaxies. This is reinforced by the fact that most of the cases where $\epsilon_{moments} \gg \epsilon_{model}$ are close-to-face-on barred galaxies. We are primarily interested in the effect of

---

[1] Column names from the SDSS table are reported in italics.

Table 1. The local sample of clusters and results of the KS tests.

ACO	RA (J2000)	Dec. (J2000)	z	r (mag)	R (arcsec)	N_{parent}	N_{RS}	$N_{\epsilon \geq 0.4}$	$N_{\text{RS}, \epsilon \geq 0.4}$	P_{parent}	P_{RS}	$P_{\epsilon \geq 0.4}$	$P_{\text{RS}, \epsilon \geq 0.4}$
(1)	(2)	(3)	(4)	(5)	(6)	(7)	(8)	(9)	(10)	(11)	(12)	(13)	(14)
16	0:16:46.30	6:44:39.84	0.084	19.88	16.09	416	185	187	99	0.875	**0.031**	0.752	0.656
168	1:15:9.79	0:14:50.64	0.045	18.48	28.52	330	181	148	84	0.959	0.846	0.854	0.555
1035	10:32:7.20	40:12:33.12	0.080	19.77	16.80	461	194	207	94	0.574	0.459	0.147	0.212
1186	11:13:51.36	75:23:39.84	0.079	19.75	16.95	311	152	128	63	0.395	0.950	0.533	0.408
1190	11:11:46.32	40:50:41.28	0.079	19.75	16.89	358	224	162	112	0.754	0.159	0.365	0.211
1367	11:44:29.52	19:50:20.40	0.021	16.83	58.29	284	206	118	87	0.161	0.219	0.149	0.076
1650	12:58:46.32	−1:45:10.80	0.085	19.90	15.97	461	290	220	138	0.239	0.649	**0.006**	0.117
1656	12:59:48.72	27:58:50.52	0.023	16.99	54.13	468	362	197	153	**0.046**	0.105	**0.004**	**0.010**
1775	13:41:55.68	26:21:53.28	0.072	19.54	18.38	456	234	202	102	0.824	0.962	0.714	0.692
1795	13:49:0.48	26:35:6.72	0.062	19.20	21.14	421	220	176	85	0.240	0.340	0.307	0.633
1904	14:22:7.92	48:33:22.32	0.071	19.49	18.76	442	252	204	118	0.902	0.314	0.912	0.233
2029	15:10:58.80	5:45:42.12	0.077	19.68	17.43	558	285	260	129	0.381	0.825	0.535	0.578
2065	15:22:42.72	27:43:21.36	0.072	19.54	18.40	567	305	263	140	0.414	0.483	0.206	0.424
2142	15:58:16.08	27:13:28.56	0.090	20.04	15.10	646	405	281	158	0.708	0.092	0.442	0.426
2151	16:5:14.88	17:44:54.60	0.037	18.04	34.41	355	189	168	86	0.305	0.460	0.254	0.143
2199	16:28:36.96	39:31:27.48	0.030	17.59	41.80	327	201	145	80	0.847	0.527	0.827	0.529
2244	17:2:43.92	34:2:48.48	0.099	20.27	13.82	556	301	247	133	0.573	0.873	0.172	0.361
2255	17:12:30.96	64:5:33.36	0.081	19.80	16.61	636	398	294	186	0.346	0.262	0.727	0.797
2256	17:3:43.44	78:43:2.63	0.060	19.12	21.82	528	341	217	138	0.317	0.137	0.752	0.412
2670	23:54:10.08	−10:24:18.00	0.076	19.66	17.56	471	250	206	109	0.474	0.676	0.974	0.169
Reference	–	–	–	–	–	9052	5175	4030	2294	–	–	–	–

Column (1): cluster ID (Abell et al. 1989). Column (2): right ascension in degrees and decimal. Column (3): declination in degrees and decimal. Column (4): cluster redshift from Ebeling et al. (1996) or from Abell et al. (1989) when available. Column (5): magnitude cut adopted, SDSS r band. Column (6): cut in the projected distance, corresponding to 1.5 Mpc. Column (7): number of galaxies in the parent sample. Column (8): number of galaxies in the RS. Column (9): number of flat ($\epsilon \geq 0.4$) galaxies in the parent sample. Column (10): number of flat ($\epsilon \geq 0.4$) galaxies in the RS. Column (11): probability that the parent sample has the same ϵ distribution as the corresponding RC. Column (12): probability that the RS has the same ϵ distribution as the corresponding RC. Column (13): probability that the sample of flat ($\epsilon \geq 0.4$) galaxies has the same ϵ distribution as the corresponding RC. Column (14): probability that the sample of flat ($\epsilon \geq 0.4$) RS galaxies has the same ϵ distribution as the corresponding RC. Probability values $P < 0.05$ are highlighted in boldface characters (see Sections 3.1 and 3.3).
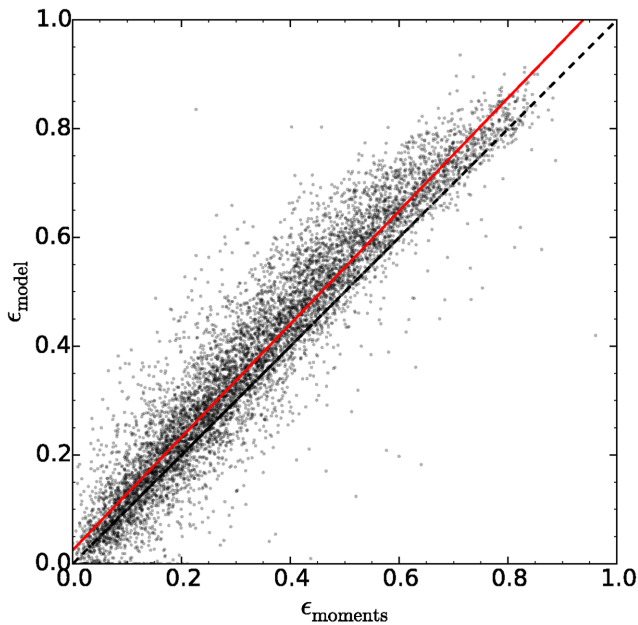

Figure 1. Comparison between ϵ_{model} and $\epsilon_{\text{moments}}$, measured in the r' band as described in the text. The solid red line is the best-fitting linear relation, while the black dashed line is the 1:1 relation. ϵ_{model} is on average higher than $\epsilon_{\text{moments}}$. (A colour version of this figure is available in the online version.)

the cluster environment on the shape of galaxies. Since this effect is larger at larger galactic radius, we choose to use ϵ_{model} as a measure of the shape of galaxies. See Appendix A for a comparison with the results using $\epsilon_{\text{moments}}$.

We investigate the variation of ϵ as a function of two different tracers of the environment density, the projected cluster-centric radius R and the projected number density of galaxies Σ_3. The latter was measured for each galaxy inside the circle on the sky comprising its three closest neighbours (e.g. Cappellari et al. 2011b).

2.2 RS determination

For each cluster, we constructed the $g' - r'$ versus r' colour–magnitude diagram (CMD). In order to reject any outliers and artefacts, we eliminated all the points in the CMD with $g' - r' \notin [0.0, 2.5]$ and galaxies with errors in $g' - r'$ greater than 0.1.

We identified the RS using the Gaussian mixture model of Houghton et al. (2012). The algorithm fits two superimposed Gaussian models: one for the RS and one for the underlying galaxy distribution, including background and foreground objects. The mean $\langle g' - r' \rangle$ of the RS Gaussian is allowed to vary linearly with the magnitude r', i.e. $\langle g' - r' \rangle = m(r' - 16) + c$, where m and c are constants to be determined. The amplitude and the dispersion Δ of the Gaussian are held constant with r'. For the background Gaussian, all parameters are independent of r'.

The algorithm determines the most likely values of m, c and Δ. In addition, it returns the probability $P(\text{RS})$ that each galaxy on the CMD belongs to the RS, and we define galaxies with $P(\text{RS}) > 0.05$
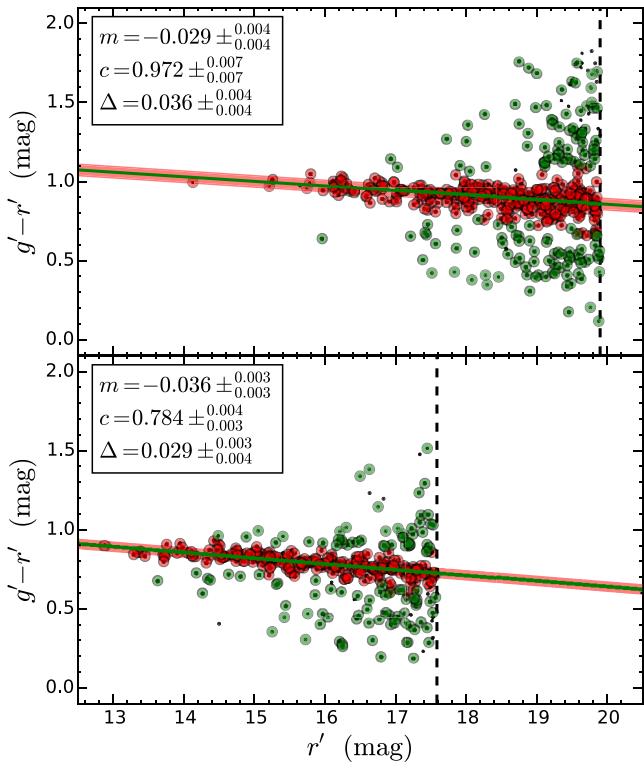
Figure 2. Two example CMDs for Abell 1650 at $z = 0.08$ (top) and Abell 2199 at $z = 0.03$ (bottom). Galaxies are marked by black dots. Red and Green circles are overlaid on RS galaxies and to non-RS galaxies. Naked dots denote galaxies with large errors that were not used in the fit. The best fit to the RS is the green line, while the region shaded in red represents the intrinsic scatter. The vertical dashed line is the adopted magnitude cut. The best-fitting parameters are reported in the top-left box (m is the slope, c the intercept and Δ the intrinsic scatter). (A colour version of this figure is available in the online version.)

to be members of the RS. This corresponds to a 2σ selection. After applying this procedure to all the 20 clusters in the sample, the average results are $\langle m \rangle = -0.037 \pm 0.006$ and $\langle \Delta \rangle = 0.035 \pm 0.007$.

In Fig. 2, we show the CMD of two clusters, Abell 1650 at $z = 0.08$ (top panel) and Abell 2199 at $z = 0.03$ (bottom panel). Each black dot represents a galaxy from the SDSS catalogue, but only the dots with an overlaid circle have been considered for the purpose of the RS determination. Red circles mark RS galaxies, while green circles mark non-RS galaxies, as determined by their value of $P(RS)$. The vertical dashed line is the magnitude cut for the cluster, while the solid green line represents the best fit to the RS, i.e. the line of equation $g' - r' = m(r' - 16) + c$. In the top-left box of each panel, we report the best-fitting value of m, c and Δ with the corresponding 1σ confidence interval.

We constructed a reference cluster (RC) as the union of all the clusters in the sample, and further constructed a reference RS as the union of all the RS's of all the clusters. The RC consists of 9052 galaxies and the reference RS sample counts 5175 entries (see the last row in Table 1, columns 7 and 8).

2.3 Redshift selection

A colour selection can be useful to reject interlopers, but it is not as reliable as a spectroscopic selection. Individual cluster galaxies can be significantly bluer than allowed by the RS (for instance, if
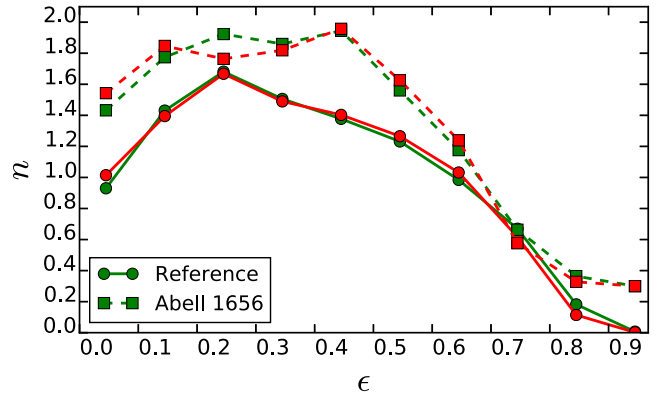
Figure 3. Distribution of projected ϵ for the RC (solid green line) and the reference RS (solid red line). The dashed lines show the distribution for Abell 1656, with the same colour coding. According to a KS test (Table 1), Abell 1656 has a different ϵ distribution than the RC. This is true also for the RS. The distributions are normalized so that the integral is unity, but the values of n for Abell 1656 are plotted 0.3 higher for display purposes. (A colour version of this figure is available in the online version.)

they are undergoing star formation). On the other hand, a number of physical processes can affect the colour of interlopers, placing them close to or on the RS (dust reddening, star formation). In order to assess the number of interlopers still present in the RS sample, we used spectroscopic data from SDSS DR10. Unfortunately, only Abell 1656 had enough candidate galaxies with spectra; therefore, the spectroscopic sample is limited to one cluster. We retrieved the redshift z for all the galaxies in the photometric sample, and rejected all the galaxies with $z < 0.01$ or $z > 0.04$ (Price et al. 2011). The sample for Abell 1656 is reduced from 468 to 387 galaxies, while the RS is reduced from 362 to 333 members. The number of interlopers is 61 and 21 for the full sample and for the RS, respectively, corresponding to a fraction of 0.14 and 0.06. We then assumed that all of the galaxies with no redshift measurement in the data base are interlopers too (20 and 8 galaxies for the full sample and for the RS, respectively). This gives a maximum fraction of interlopers of 0.18 and 0.08.

3 RESULTS

We start this section studying if $n(\epsilon)$ varies between different clusters, and the properties of the RS sample (Section 3.1). We then study the redshift selected sample of Abell 1656 to study the effect of interlopers (Section 3.2). In Section 3.3, we consider again the full sample, where we repeat the analysis for intrinsically flat galaxies. We then study the relation between ϵ and r'-band luminosity (Section 3.4) and conclude this section by studying a subsample of morphologically selected galaxies (Section 3.5) and splitting our sample according to the shape of the luminosity profile (Section 3.6).

3.1 Full sample

In Fig. 3, we plot $n(\epsilon)$ of the RC (solid green line), alongside the distribution of the reference RS (solid red line). Each distribution has been normalized so that its integral between $\epsilon = 0$ and 1 is unity. For both the RC and the RS, we find an average ellipticity $\langle \epsilon \rangle = 0.38 \pm 0.01$ and a standard deviation $\sigma_\epsilon = 0.21 \pm 0.01$.

We then used a Kolmogorov–Smirnov (KS) test on the null hypothesis that any individual cluster in the sample has the same $n(\epsilon)$

as the RC, and that any of the cluster RS has the same $n(\epsilon)$ as the reference RS. The results are summarized in Table 1. For each cluster, we list the number of galaxies found inside the adopted SDSS aperture (column 7) and the number of galaxies on the RS (column 8). We then report the results of the KS test: for each cluster we list the probability that its $n(\epsilon)$ is the same as the RC (column 11), and that $n(\epsilon)$ of its RS is the same as the reference RS (column 12). We have only one entry with $P \lesssim 0.05$ for both columns 11 and 12 (Abell 1656 and Abell 16, respectively). If we assume that $n(\epsilon)$ is the same between all clusters, we expect the results of the KS test to be distributed uniformly between 0 and 1. We performed an Anderson–Darling (AD; Anderson & Darling 1954) uniformity test for the null hypothesis that the values of columns 11 and 12 of Table 1 are drawn from the uniform distribution. The AD values are 0.48 and 0.41 for columns 11 and 12, respectively, corresponding to p-values $\gg 0.25$ (Rahman, Pearson & Heien 2006). Therefore, there is no evidence of any difference between the $n(\epsilon)$ of our sample of clusters.

Next we studied the variation of ϵ with the cluster-centric radius R.

In Fig. 4, we plot ϵ for nine bins in log R. The green diamonds mark each bin from the parent sample in the CMD, and the red circles mark ϵ for the galaxies on the RS. At the top of each panel, the numbers in parentheses are the numbers of RS galaxies in each bin (we eliminated any bin with less than three galaxies). The error bars were derived assuming that for each bin in log R, the distribution $n(\epsilon)$ is flat between $\epsilon = 0$ and 1, and zero otherwise. Such a distribution has standard deviation $1/\sqrt{12}$; therefore, the error on the mean ϵ for each bin is $1/\sqrt{12\,N}$, where N is the number of galaxies in that bin. Since $n(\epsilon)$ is hardly flat, and does not extend to $\epsilon = 1$ (Fig. 3), it follows that our estimate of the error is a conservative one. The box in the bottom-left corner reports the slope (with errors) of the best linear fit, using least-squares minimization. The uncertainties on the slopes were derived from the error bars; therefore, they too represent a conservative estimate. The top panel depicts the results for the RC: both the parent and RS sample show a clear trend of ϵ with log R, in that the best-fitting slope is more than three standard deviations away from 0. For brevity, we call the observed trend the ellipticity–radius relation (ϵ–R). The central panel shows the same plot for Abell 1650, a cluster where the ϵ–R trend is clearly present. In contrast, Abell 2142 (bottom panel) is an example of a cluster where the relation is not detected, i.e. the measured slope is within three standard deviations of 0. For the parent samples, four clusters have a slope that is more than 3σ from 0, including Abell 1650. Nine clusters have slopes between 1σ and 3σ above 0, and seven clusters (including Abell 2142) have a slope that is within 1σ from 0 (this includes Abell 16 and Abell 168, which have negative slopes). The breakdown is 4/9/7. For the RS samples, the breakdown is 5/10/5 (Abell 16 and Abell 168 still have negative slopes). In all clusters, the best-fitting slope of the parent sample and that of the RS sample are statistically consistent to the level of 3σ.

To estimate the probability that our result arises from chance, we assume Gaussian errors on the best-fitting slope and use the binomial distribution:

$$f(k; n, p) \equiv \binom{n}{k} p^k (1-p)^{n-k}. \tag{1}$$

The probability that out of 20 best-fitting slopes 13 are more than 1σ above 0 is $f(13, 20, 0.16) \approx 1 \times 10^{-6}$. We therefore conclude that the observed ϵ–R relation is a real effect.

We find no correlation between the value of the best-fitting slope and global cluster parameters, like X-ray temperature or X-ray lu-
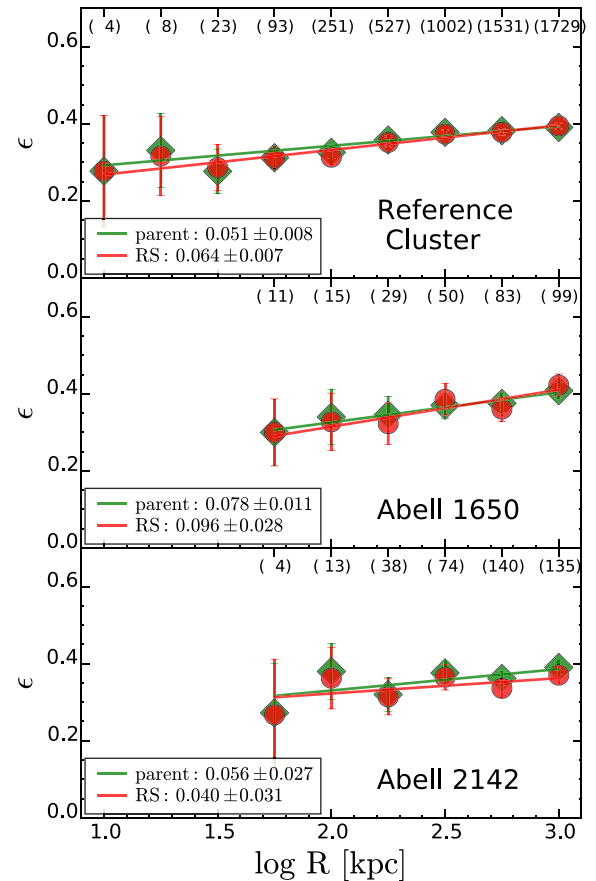

Figure 4. The projected ellipticity ϵ of galaxies as a function of the projected cluster-centric radius. The RC is shown at the top, followed by two example clusters: Abell 1650 (centre) and Abell 2142 (bottom). The green diamonds represent all galaxies in the cluster; red circles represent RS galaxies only. The boxes in the bottom-left corners report the best-fitting slope to the points and associated errors. The reference sample, as well as Abell 1650, shows a trend of ϵ with log R, which we call the ϵ–R relation. In Abell 2142, the trend is not significant (the slope is less than three standard deviations above 0). The numbers in parentheses are the number of galaxies in each bin of log R for the RS. (A colour version of this figure is available in the online version.)

minosity (Ebeling et al. 1996), richness (Abell et al. 1989) or Bautz–Morgan type (Bautz & Morgan 1970).

3.2 Spectroscopic sample for Abell 1656

In Section 2.3, we presented a sample of redshift selected cluster member for Abell 1656. The ϵ–R relation stays the same for the original sample (Fig. 5, top panel) and for the redshift selected sample (Fig. 5, bottom panel). The significance of the trend increases for both the parent sample and the RS, but the trends are statistically consistent. If anything, the slope of the best-fitting relation increases going from the original sample to the spectroscopic sample.

3.3 Flat galaxies

We repeated the analysis for the subset of flat galaxies. Emsellem et al. (2011) showed that there are no SRs flatter than $\epsilon \gtrsim 0.4$ (we treat double sigma galaxies as FRs; Krajnović et al. 2011). Therefore, we isolate a sample of intrinsically flat galaxies by selecting
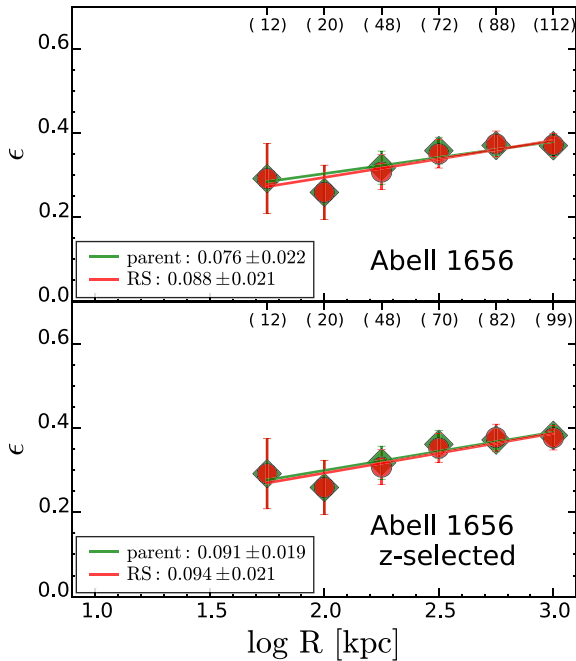
Figure 5. Same as Fig. 4, for the Abell 1656 sample (top panel) and for the sample of redshift selected cluster members (bottom panel; see Section 2.3). The trend of ϵ with cluster-centric radius R observed in Abell 1656 is not an effect of interlopers: the slope of the best-fitting linear relations is statistically consistent between the original sample and the redshift selected samples (boxes in the bottom-left corner of each panel). (A colour version of this figure is available in the online version.)

Figure 6. The projected ellipticity ϵ of galaxies as a function of the projected cluster-centric radius. The RC is shown at the top and the reference RS sample in the bottom panel. In each plot, the blue ellipses represent galaxies that appear flat on the sky ($\epsilon \geq 0.4$). The magenta circles represent galaxies that appear round on the sky ($\epsilon < 0.4$). The blue and magenta lines are least-squares best fits to the data; their slopes are reported in the bottom-left corner of each figure. The numbers in parentheses are the number of galaxies in each bin of log R for the flat subsample. (A colour version of this figure is available in the online version.)

$\epsilon \geq 0.4$.[2] We performed a KS test comparing the flat galaxies in the RC to those in each single cluster. We then repeated the test for RS galaxies only. The results are listed in Table 1 (columns 13 and 14). We find that Abell 1656 fails both tests and Abell 1650 fails one test. To test the null hypothesis that the values in columns 13 and 14 are distributed uniformly between 0 and 1, we use again the AD uniformity test. The resulting values are 0.53 and 1.84 for columns 13 and 14, respectively, corresponding to p-values $\gg 0.25$ and $0.10 < p-$value < 0.15. We infer that there is no conclusive evidence to suggest that the distribution of ϵ is different between different clusters, as we cannot reject the null hypothesis with confidence greater than $P = 0.01$.

However, by looking at Abell 1656 in Table 1, we see that this cluster scores very low confidence in three out of four tests (columns 11, 13 and 14). Since these values are not independent, as a conservative estimate we adopt the largest one as the probability that the $n(\epsilon)$ of Abell 1656 is the same as the $n(\epsilon)$ of the RC, $P(\text{same}) \leq 0.05$.

We now look into the relation of ϵ with the cluster-centric radius R. The top panel of Fig. 6 shows the ϵ–R relation for the subsample of flat galaxies. The magenta circles are galaxies with $\epsilon < 0.4$ (binned in log R), and the blue ellipses are galaxies with $\epsilon \geq 0.4$. The trend is observed for both the round and flat subsamples; however, the ϵ–R relation for flat galaxies (0.035 ± 0.005) is both steeper and statistically more significant than that of round galaxies (0.014 ± 0.003). The bottom panel of Fig. 6 shows the same relation for galaxies on the RS: the best-fitting slope for flat galaxies

is consistent with the previous one. The change in mean ϵ for flat galaxies is $\Delta \epsilon \approx 0.1$ over the observed range in log R.

If we repeat our analysis substituting log R with log Σ_3, we find equivalent results: ϵ decreases with log Σ_3. This is a consequence of the anticorrelation between R and Σ_3. At this stage, it is not possible to disentangle which relation is more fundamental.

3.4 Dependence on luminosity

In Fig. 7, we show how the RC populates the ϵ versus M_r space. The colour bar represents the log number density of galaxies. We notice that there is an excess of round, luminous galaxies at $M_r \approx -23$ mag (Fig. 7, bottom-left corner). In contrast, there are only 31/9052 galaxies with $\epsilon \geq 0.4$ and $M_r \leq -22$ mag, and only 2/9052 galaxies with $\epsilon \geq 0.4$ and $M_r \leq -23$ mag. It is possible that a number of these are foreground interlopers. The brightest of these galaxies is however the cD galaxy of Abell 1650, which is genuinely flat. For $M_r \lesssim -22$ mag, the contour lines indicate a gradual increase of ϵ with decreasing r'-band luminosity.

In Fig. 8, we show ϵ for nine bins in M_r, for the RC as well as for the reference RS (top panel). For galaxies with -22 mag $\lesssim M_r \lesssim -19$ mag, there seems to be no dependence of ϵ with M_r. However, galaxies more luminous than ≈ -23 mag are on average rounder. In the middle and bottom panel of Fig. 8, we plot ϵ against M_r for the RC and for the reference RS, respectively, but this time we divide each sample into two subsets at $\epsilon = 0.4$. Flat galaxies do not present a trend of ϵ with magnitude, and the slope of the best-fitting relation is statistically consistent with zero.

---

[2] Notice that this biases our sample against FRs with lower intrinsic ellipticity, because the range of possible inclinations that satisfy the constraint $\epsilon \geq 0.4$ decreases with decreasing intrinsic ellipticity.
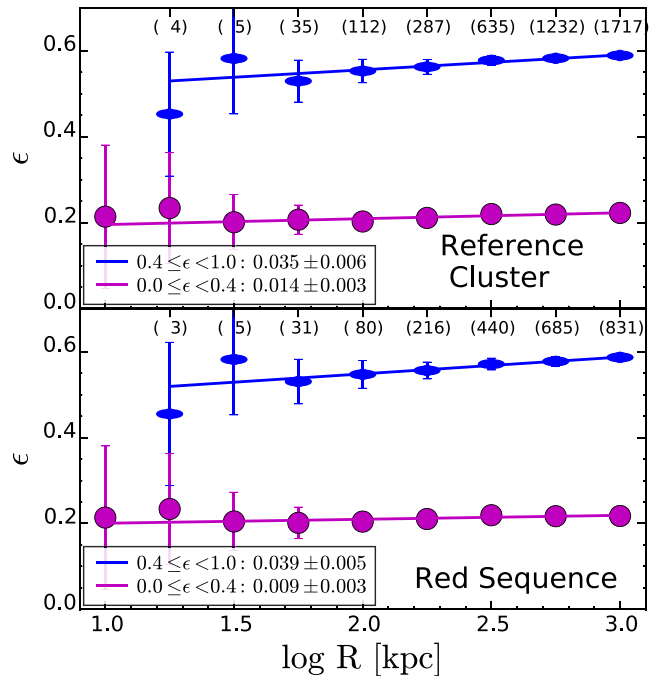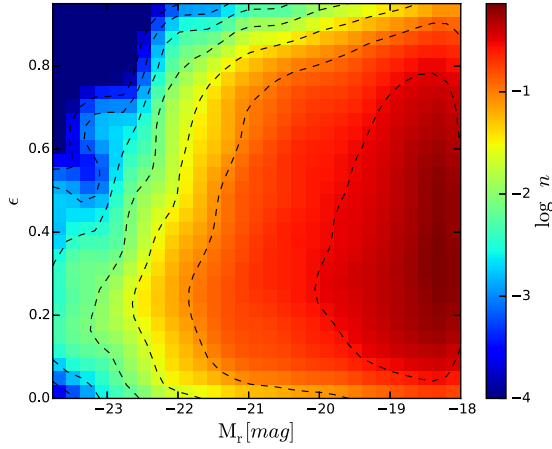
Figure 7. The distribution of the galaxies (RC) in the magnitude–ϵ plane. n is the number density of galaxies in the $\epsilon - M_r$ space. There is an excess of round, luminous galaxies ($M_r \lesssim -22$ mag, bottom-left corner). (A colour version of this figure is available in the online version.)
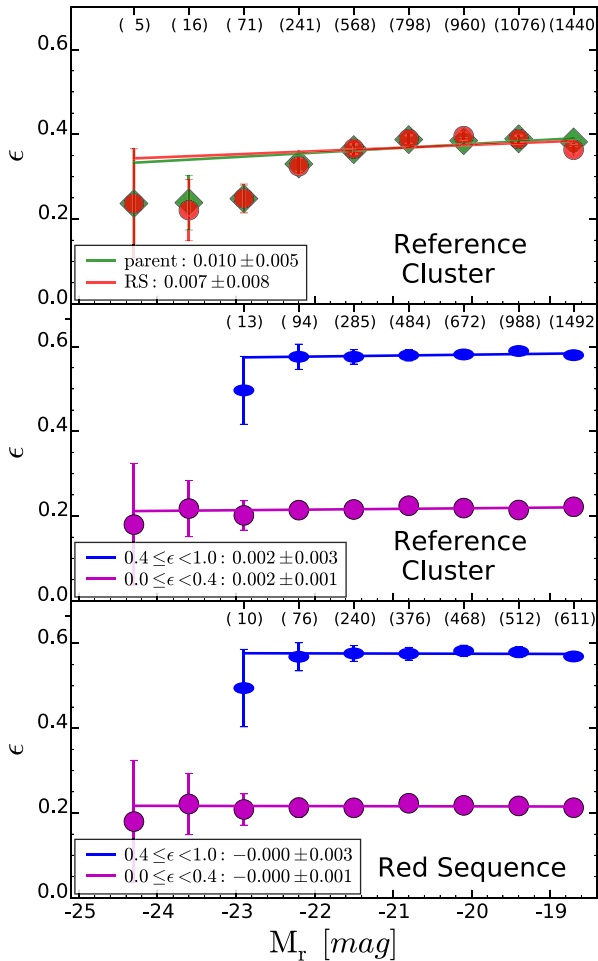

Figure 8. Top panel: ϵ versus M_r for the RC (green diamonds) and for the RS (red circles). Galaxies more luminous than $M_r \approx -23$ mag are on average rounder than the galaxies with $M_r \gtrsim -23$ mag. Middle and bottom panel: same as Fig. 6, but showing ϵ as a function of M_r for $\epsilon < 0.4$ and for $\epsilon \geq 0.4$. When we consider the subsample of flat galaxies ($\epsilon \geq 0.4$), there is no trend of ϵ with M_r. This is quantified by the slope of the best-fitting linear relation, which is statistically consistent with zero (bottom-left corner of each panel). (A colour version of this figure is available in the online version.)

Table 2. The ϵ–R relation at fixed r'-band absolute magnitude (see Section 4.2).

M_r (1)	$m_{\rm parent}$ (2)	$\dfrac{m_{\rm parent}}{\sigma_{\rm parent}}$ (3)	$m_{\rm RS}$ (4)	$\dfrac{m_{\rm RS}}{\sigma_{\rm RS}}$ (5)
$M_r \leq -22$	0.094	2.3	0.089	2.6
$-22 < M_r \leq -21$	0.024	3.5	0.028	2.2
$-21 < M_r \leq -20$	0.038	1.5	0.058	2.1
$-20 < M_r \leq -19$	0.034	2.9	0.060	4.4
$-19 < M_r \leq -18$	0.067	6.5	0.090	10.0

Column (1): magnitude interval (r'-band absolute magnitude). Column (2): the measured slope for the ϵ–R relation. Column (3): significance on the measured slope for the ϵ–R relation (in units of the uncertainty σ). Column (4): the measured slope for the ϵ–R relation for RS galaxies only. Column (5): significance on the measured slope for the ϵ–R relation for RS galaxies only (in units of the uncertainty σ).

Next we studied the ϵ–R relation by dividing the sample into luminosity bins. The ϵ–R relation persists, but decreases in significance when we decrease the sample size. The results are listed in Table 2. We report the adopted magnitude interval (column 1), the measured best-fitting slope (column 2) and the significance of the ϵ–R relation in that interval (column 3). We also list the best-fitting slope for the RS (column 4) and the significance of the ϵ–R relation for the RS (column 3). The significance of the ϵ–R relation is the ratio of the best-fitting slope m to its uncertainty σ. In general, the ϵ–R relation is recovered in each magnitude bin; however, the strongest slope and the highest significance are found for the least luminous galaxies.

3.5 GZ2 morphological selection

GZ2 is a citizen science project providing morphological classifications for $\approx 300\,000$ galaxies drawn from the SDSS sample. Cross-correlating their catalogue with our sample we find 1425 matches (≈ 16 per cent). We used debiased likelihoods to identify smooth objects ($P_{\rm smooth} \equiv t01\_smooth\_or\_features\_a01\_smooth\_debiased$). Objects with $P_{\rm smooth} > 0.8$ correspond to ETGs in the Hubble classification (Willett et al. 2013). However, this selection leaves us with 252 galaxies, of which only 50 are flat ($\epsilon \geq 0.4$). This is insufficient to constrain the slope of the ϵ–R relation ($m = 0.065 \pm 0.036$, see Fig. 9, top panel).

If we relax the above condition and use instead $P_{\rm smooth} > 0.5$ and $P_{\rm spiral} < 0.5$, we find 676 galaxies (and 204 flat galaxies). In the bottom panel of Fig. 9, we show that the ϵ–R relation still holds for flat, smooth galaxies, albeit only to the 2σ level (the best-fitting linear slope is $m = 0.033 \pm 0.016$). This is statistically consistent with the trend without morphological selection ($m = 0.035 \pm 0.006$). Therefore, it appears that the spiral contamination is not the driving mechanism behind the observed relation.

3.6 Luminosity profile

An alternative method to classify galaxies is to use the shape of the luminosity profile as a function of radius. Following Vincent & Ryden (2005), we used *fracDeV* to divide the RC into four subsets: galaxies with $0 < =fracDeV < 0.1$ ($n \lesssim 1.2$) are 'ex' galaxies, galaxies with $0.1 < =fracDeV < 0.5$ ($1.2 \lesssim n \lesssim 2.0$) are 'ex/de' galaxies. Conversely, 'de/ex' galaxies have $0.5 < =fracDeV <$
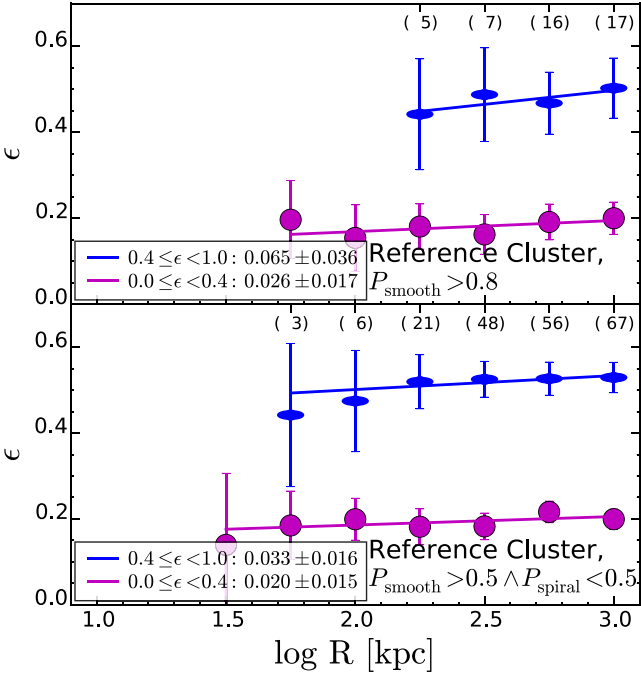
Figure 9. Same as Fig. 6, but for the subsample of cluster galaxies morphologically classified as smooth in GZ2. In each plot, the blue ellipses represent galaxies that appear flat on the sky ($\epsilon \geq 0.4$). The magenta circles represent galaxies that appear round on the sky ($\epsilon < 0.4$). The blue and magenta lines are least-squares best fits to the data; their slopes are reported in the bottom-left corner of each figure. The numbers in parentheses are the number of galaxies in each bin of log R for the flat subsample. The top panel shows the results for the subsample of galaxies with $P_{\mathrm{smooth}} > 0.8$, but it does not have enough galaxies to constrain the slope. The bottom panel shows the results with a more generous selection $P_{\mathrm{smooth}} > 0.5$ and $P_{\mathrm{spiral}} < 0.5$. (A colour version of this figure is available in the online version.)

0.9 ($2.0 \lesssim n \lesssim 3.3$) and finally 'de' galaxies have $fracDeV > = 0.9$ ($n \gtrsim 3.3$).

In Fig. 10, we plot the ϵ–R relation for the RC, splitting the galaxies according to their light profile. For flat ex galaxies, the best-fitting slope shows that there is no evidence of correlation between ϵ and log R (top panel). For flat ex/de galaxies, there is marginal evidence for a trend (the slope of the best-fitting linear relation is 2σ above 0, second panel). For flat de/ex and de galaxies, the significance increases to 5σ (third and bottom panels). The fraction of flat ex and ex/de galaxies increases with log R (numbers in parentheses). This trend, combined with the fact that ex and ex/de galaxies are on average a little flatter than de/ex and de galaxies, contributes to the ϵ–R relation observed for the undivided RC (see Section 3.1).

4 DISCUSSION

We have shown that in rich clusters ϵ depends on radius. We find that galaxies closer to the cluster centre are on average rounder. The ϵ–R relation persists when considering only galaxies with $\epsilon \geq 0.4$. In the next section, we evaluate the effect of observational bias and establish that the trend is indeed genuine. We then evaluate the effect of the luminosity (Section 4.2) and of the T–Σ relation (Section 4.3). Finally, we discuss two related works (Section 4.4) and proceed to review the possible explanations for the observed relation (Section 4.5).
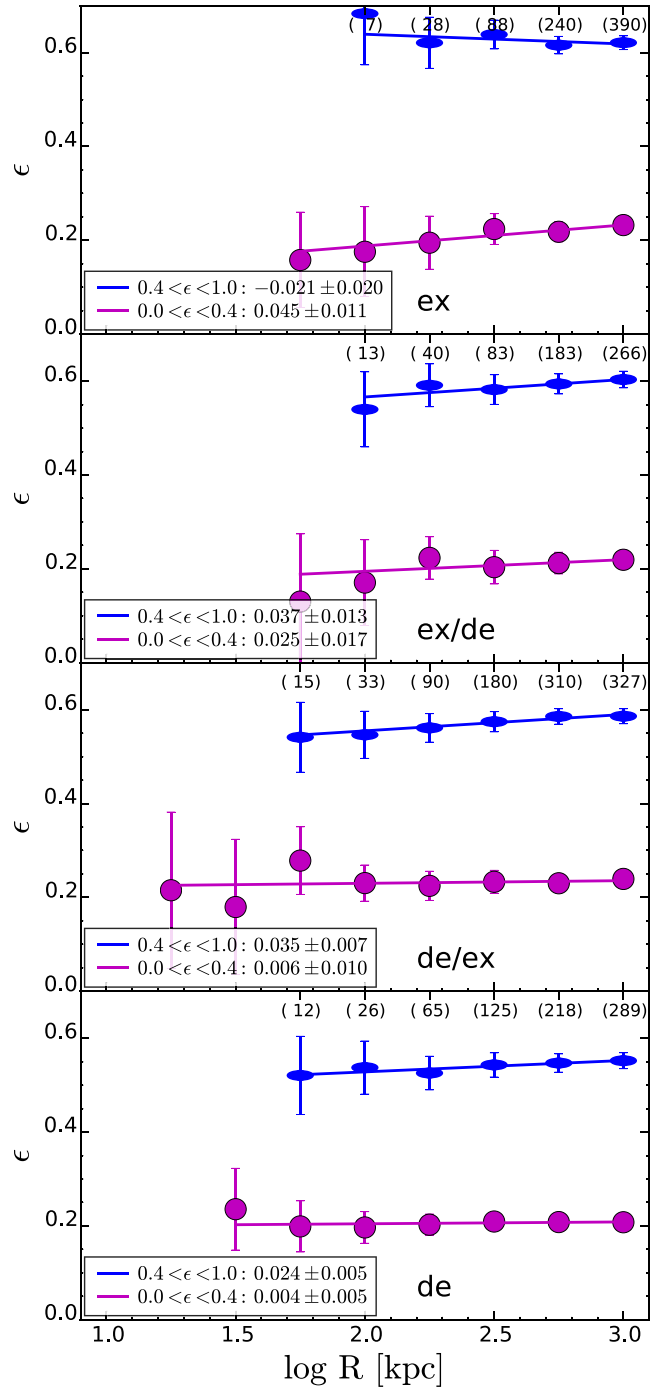
Figure 10. Same as Fig. 6, but here we split the sample according to the shape of the luminosity profile. For flat galaxies, the trend of increasing ϵ with log R is recovered for de/ex and de galaxies (third and fourth panels). For flat ex/de galaxies, there is only marginal evidence of a trend (second panel), while no significant trend is observed for flat ex galaxies (top panel). See Section 3.6 for the definition of the labels. (A colour version of this figure is available in the online version.)

4.1 Observation bias

The value of ϵ is already corrected for PSF effects, because the model for the light profile is convolved with the relevant PSF. To evaluate any residual PSF effect, we conduct two tests. We repeated our analysis using $\epsilon_{\mathrm{moments}}$ instead of $\epsilon_{\mathrm{model}}$ (as in e.g. KR05).

$\epsilon_{\text{moments}}$ was corrected for PSF effects according to the prescription of Bernstein & Jarvis (2002). Given that ϵ_{model} is systematically higher than $\epsilon_{\text{moments}}$, it is not surprising that our result changes. However, the observed trends are still present (see Appendix A). As a further test for the effect of the PSF, we repeated our analysis limiting our sample to well-resolved objects (where $\tau/\tau_{\text{PSF}} >$ 6.25; see KR05). The ϵ–R relation persists even for these galaxies where the effect of the PSF is negligible, with lower significance as expected from the smaller sample size.

Finally, we remark that the PSF would make all galaxies appear rounder, affecting smaller galaxies more than larger ones. This means that in order for PSF effects to cause or enhance the ϵ–R relation, smaller galaxies would need to be a larger fraction of the population at small R, but the opposite is true (Dressler 1980; Hogg et al. 2004).

All of our samples include a number of interlopers, foreground or background galaxies which are not gravitationally bound to the relevant cluster. This is true both for the parent sample and (to a lesser extent) for the RS sample. To understand the possible effect of interlopers on the observed trend of ϵ versus log R, we consider the following scenario. For a given cluster, we assume that interlopers are distributed uniformly across the sky. In contrast, the density of cluster member galaxies is higher in the centre and decreases at larger radii. This means that the fraction f of interlopers over the sample increases with log R. If interlopers had a higher average ϵ than cluster members, then the observed variation of ϵ with log R would be a consequence of the variation of f with log R. For Abell 1656, this scenario is ruled out by the fact that the ϵ–R relation holds even for the sample of spectroscopically confirmed cluster members (Section 3.2). In addition, the 61 interlopers have an average ellipticity $\epsilon = 0.34 \pm 0.19$, lower than the value for cluster members. As expected, the fraction of interlopers increases with log R. If interlopers have a lower-than-average ϵ for the other clusters too, then their inclusion cannot artificially create the observed ϵ–R relation, but rather acts to mask it.

4.2 The effect of luminosity

More luminous galaxies are both rounder and more common in the densest environments (Dressler 1980; Hogg et al. 2004). Could the ϵ–R relation arise from this trend? This hypothesis is contradicted by the fact that for the flat subsample there is no trend of ϵ with M_r (Fig. 8), but for the same galaxies a clear correlation exists between ϵ and log R. In addition, the trend of ϵ with log R is observed even at fixed magnitude, and is stronger for the less luminous galaxies (Table 2).

4.3 The morphology–density relations

The final source of bias that we consider is the T–Σ relation (Dressler 1980). Es, S0s and spiral galaxies have different ϵ distributions. Therefore, the trend of their number fraction with local environment affects systematically the overall ϵ distribution. In order to quantify this effect, we need Hubble morphological classifications for all the galaxies, but these are not available.

In Section 3.3, we divided the RC (and the reference RS) into a flat ($\epsilon \geq 0.4$) and a round subsample ($\epsilon < 0.4$). The subset of round galaxies contains both SRs (regardless of their inclination on the sky) and close-to-face-on discs. Therefore, the observed trend of increasing flattening with log R can be due to the decreasing fraction of SRs (Cappellari et al. 2011b; D'Eugenio et al. 2013; Houghton et al. 2013; Fogarty et al. 2014; Scott et al. 2014) and/or to a change

in the intrinsic shape of galaxies. Without a dynamical classification for each galaxy, it is impossible to draw any conclusions from the observed trend.

However, the subset of galaxies with $\epsilon \geq 0.4$ does not contain SRs (which are intrinsically round). Therefore, the observed trend of increasing projected ellipticity with radius arises because flat galaxies have lower intrinsic ellipticity nearer to the centre of clusters. Flat galaxies include both FR ETGs and spiral galaxies. If these two classes have different $n(\epsilon)$, the ϵ–R relation could result from a trend of the morphological fractions with cluster-centric radius. However, it seems that on average FR ETGs have the same intrinsic flattening as spiral galaxies (Weijmans et al. 2014), a fact that undermines the above explanation. Nevertheless in Section 3.5 we attempted to remove spiral galaxies: we used GZ2 data to select a sample of smooth objects. When we adopt the condition $P_{\text{smooth}} >$ 0.8, we find 252 galaxies, of which only 50 are flat ($\epsilon \geq 0.4$). The slope of the ϵ–R relation for flat galaxies is 1.8 standard deviations above 0 (Fig. 9, top panel). For a sample of 50 flat galaxies selected randomly from the RC, we expect the slope to be 0.6 standard deviations away from 0. This suggests (but does not demonstrate) that the low significance of the ϵ–R relation of smooth, flat galaxies is due to insufficient sample size, as opposed to the systematic removal of the galaxies with $P_{\text{smooth}} \leq 0.2$. We then relaxed the morphological selection, finding 676 galaxies, of which 204 are flat (we used $P_{\text{smooth}} > 0.5$ and $P_{\text{spiral}} < 0.5$, see again Section 3.5). In this case, the slope of the ϵ–R relation of flat galaxies was 2.1 standard deviations above 0. For a sample of 204 flat galaxies randomly selected from the RC, we expected the slope to be 1.3 standard deviations above 0. The fact that we find a value of 2.1 suggests again that the low significance is due to the sample size rather than to any systematic effect. In addition, the slope is statistically consistent with what found in Fig. 6, even though a significant number of spiral galaxies have been removed.

Willett et al. (2013) cross-correlated the GZ2 catalogue with a professionally classified sample of SDSS galaxies (Nair & Abraham 2010). They showed that galaxies classified as smooth in GZ2 ($P_{\text{smooth}} > 0.8$) are morphological ETGs for 96.7 per cent of the cases (the matching for our relaxed conditions is not covered). Therefore, it appears that the spiral contamination is not the driving mechanism behind the observed relation.

Our result could still be explained by the T–Σ relation, because within ETGs the fraction of Es increases with projected density (and nearer to the centre of clusters; Whitmore et al. 1993). Since Es are on average rounder than S0s, the ϵ–R relation could be an effect of the T–Σ relation. To investigate this possibility, we need to distinguish between Es and S0s, which cannot be done with GZ2 and is beyond the scope of this paper. But the latest view on the E/S0 divide, offered by the ATLAS[3D] survey, is that the traditional visual E/S0 morphology is flawed. Emsellem et al. (2011) demonstrated that two thirds of the locally classified Es are kinematically identical to S0s. We therefore reframe our findings within the FR/SR paradigm. 15 per cent of the local ETGs are SRs, but their fraction increases dramatically nearer to the centre of clusters (Cappellari et al. 2011b; D'Eugenio et al. 2013; Houghton et al. 2013; Fogarty et al. 2014; Scott et al. 2014). Since SRs are on average rounder than FRs, the ϵ–R relation could be a consequence of the kinematic morphology–density relation. However, by selecting galaxies with $\epsilon \geq 0.4$, we eliminate all SRs. By further imposing $P_{\text{smooth}} > 0.8$, we eliminate all spiral galaxies. The fact that the ϵ–R relation persists even for smooth galaxies flatter than $\epsilon = 0.4$ demonstrates that the ϵ–R relation is not a consequence of the kinematic morphology–density relation. The decrease of projected ellipticity ϵ nearer to the

centre of clusters implies that the distribution of *intrinsic* ellipticity changes with log R. This is evidence of the effect of the cluster and/or local environment on the shape of FRs, be they FR Es or FR S0s.

4.4 Comparison with other work

KR05 used a much larger sample of $\approx$200 000 galaxies to investigate the relation between the shape of galaxies (as expressed by the axial ratio q) and the local environment (measured by the number density of neighbour galaxies in the sky). Their sample differs from ours in that (i) they adopted a cut in apparent magnitude at $r' = 17.77$ mag and (ii) their selection is not limited to specific environments, whereas we focused on rich clusters of galaxies. These differences make it difficult to compare our results.

The noise introduced by their selection can be appreciated by looking at their tables 3–5. Despite having $\approx$20 times the sample size, the significance of the recovered trends is similar to ours. KR05 divide their sample according to the luminosity profile, as we did in Section 3.6. Our results are in qualitative agreement with theirs. However, they do not investigate the trend of intrinsically flat galaxies.

Weijmans et al. (2014) studied the intrinsic shape distribution of the ATLAS^{3D} ETGs, using IFS to separate SRs and FRs. As we have seen, they find that the intrinsic flattening of FR ETGs is consistent with that of spiral galaxies, a fact that reinforces our result. However, contrary to our findings, they do not observe any correlation of intrinsic flattening and environment (as parametrized by log Σ_3). It is unclear if this depends on the small size of their sample, and/or on the range of environments that they explore (the ATLAS^{3D} survey contains just one unrelaxed cluster, Virgo).

4.5 Possible driving mechanisms

Here we propose three possible explanations for the observed trend.

(a) We can view our result in the framework of the B/D decomposition. By definition discs are intrinsically flat, while bulges are rounder. A systematic change in the B/D mass ratio with log R could therefore account for the ϵ–R relation. We notice however that in their study of eight nearby clusters ($z < 0.06$), Hudson et al. (2010) do not find any correlation between R-band B/D light ratios and the cluster-centric radius (except for the innermost $\approx$0.3 Mpc).

(b) The cluster environment affects the stellar population of member galaxies, for example by removing cold gas from the disc and halting star formation there (see Boselli & Gavazzi 2006, for a review). We therefore expect to observe a trend between the cluster-centric radius and the photometric properties of galaxies. For instance, even at fixed B/D mass ratio, a trend in stellar age can generate a trend in the B/D light ratio, which in turn could give rise to the ϵ–R relation. This is supported by the observed correlation between disc colour and cluster-centric radius, while no such correlation is observed for bulge colour (Balogh, Navarro & Morris 2000; Hudson et al. 2010; Head et al. 2014).

(c) FRs might contain subclasses with different intrinsic ellipticity, for instance Weijmans et al. (2014) suggest the existence of a tail of rounder FRs in the ATLAS^{3D} sample. If this is correct, the ϵ–R relation for FRs could arise from the radial distribution of different classes of FRs.

(d) Cluster environments also affect the dynamical structure of galaxies. Harassment and stripping make discs smaller and thicker, therefore changing their intrinsic ellipticity. This is supported by

Houghton et al. (2013), who studied a sample of galaxies in the central 15 arcmin (radius) of the Coma Cluster. For each galaxy they measure λ (a proxy for the projected angular momentum per unit mass; Emsellem et al. 2007), and find that the maximum value of λ for Coma FRs is lower than that of FRs from the ATLAS^{3D} survey (Emsellem et al. 2011). They suggest that this is due to the cluster environment affecting the anisotropy of galaxies (Binney & Tremaine 1988).

In order to understand the origin of the ϵ–R relation, an extended IFS survey of cluster galaxies is required. The Coma Cluster is an ideal starting point. Ongoing surveys (SAMI, Croom et al. 2012, MaNGA, Bundy et al. 2015) could also address this problem, depending on their coverage of rich clusters.

5 CONCLUSION

We studied the projected ellipticity ϵ of galaxies in a sample of 20 nearby ($z < 0.1$) rich clusters and show the following.

(i) There is no evidence of differences between the distribution of ϵ among the clusters in our sample, except possibly for the Coma Cluster (Abell 1656).

(ii) There exists a correlation between ϵ and the projected cluster-centric radius R, which we refer to as the ϵ–R relation.

(iii) The ϵ–R relation exists independently of the trend of more luminous galaxies to be both rounder and more common in the centre of clusters.

(iv) The ϵ–R relation is stronger for galaxies on the RS, and persists for a redshift selected sample in the Coma Cluster.

(v) The ϵ–R relation is steeper for flat galaxies ($\epsilon \geq 0.4$; excludes SRs) than for round galaxies ($\epsilon < 0.4$; a mixture of FRs and SRs).

(vi) For flat galaxies, there is no correlation between ϵ and r'-band luminosity.

(vii) There is marginal evidence (2σ) that the ϵ–R relation persists for flat ETGs, as classified by GZ2. The low significance is likely due to the small sample size.

We concluded that the ϵ–R is evidence for physical effects causing intrinsically flat galaxies (including FR ETGs) to be rounder near to the centre of rich clusters.

Foundation and the US Department of Energy Office of Science. The SDSS-III website is http://www.sdss3.org/.

Finally, we acknowledge the work of the Galaxy Zoo 2 team and volunteers.

REFERENCES

Abell G. O., Corwin H. G., Jr, Olowin R. P., 1989, ApJS, 70, 1
Ade P. A. R. et al., 2014, A&A, 566, A54
Ahn C. P. et al., 2014, ApJS, 211, 17
Anderson T. W., Darling D. A., 1954, J. Am. Stat. Assoc., 49, 765
Balogh M. L., Navarro J. F., Morris S. L., 2000, ApJ, 540, 113
Bautz L. P., Morgan W. W., 1970, ApJ, 162, L149
Bernstein G. M., Jarvis M., 2002, AJ, 123, 585
Binney J., Tremaine S., 1988, Galactic Dynamics. Princeton Univ. Press, Princeton, NJ
Boselli A., Gavazzi G., 2006, PASP, 118, 517
Bundy K. et al., 2015, ApJ, 798, 7
Cappellari M. et al., 2007, MNRAS, 379, 418
Cappellari M. et al., 2011a, MNRAS, 413, 813
Cappellari M. et al., 2011b, MNRAS, 416, 1680
Croom S. et al., 2012, MNRAS, 421, 872
D'Eugenio F., Houghton R. C. W., Davies R. L., Dalla Bontà E. D., 2013, MNRAS, 429, 1258
de Vaucouleurs G., 1948, Ann. Astrophys., 11, 247
de Zeeuw P. T. et al., 2002, MNRAS, 329, 513
Dressler A., 1980, ApJ, 236, 351
Dressler A. et al., 1997, ApJ, 490, 577
Ebeling H., Voges W., Böhringer H., Edge A. C., Huchra J. P., Briel U. C., 1996, MNRAS, 281, 799
Emsellem E. et al., 2007, MNRAS, 379, 401
Emsellem E. et al., 2011, MNRAS, 414, 818
Fogarty L. M. R. et al., 2014, MNRAS, 443, 485
Head J. T. C. G., Lucey J. R., Hudson M. J., Smith R. J., MNRAS, 440, 1690
Hirata C., Seljak U., 2003, MNRAS, 343, 459
Hogg D. W. et al., 2004, ApJ, 601, L29
Holden B. P. et al., 2009, ApJ, 693, 617
Houghton R. C. W., Davies R. L., Dalla Bontà E., Masters R., 2012, MNRAS, 423, 256
Houghton R. C. W. et al., 2013, MNRAS, 436, 19
Hudson M. J., Stevenson J. B., Smith R. J., Wegner G. A., Lucey J. R., Simard L., 2010, MNRAS, 409, 405
Jørgensen I., Franx M., 1994, ApJ, 433, 553
Kormendy J., Bender R., 2012, ApJS, 198, 2
Kormendy J., Djorgovski S., 1989, ARA&A, 27, 235
Krajnović D. et al., 2011, MNRAS, 414, 2923
Kuehn F., Ryden B. S., 2005, ApJ, 634, 1032 (KR05)
Lambas D. G., Maddox S. J., Loveday J., 1992, MNRAS, 258, 404
Nair P. B., Abraham R. G., 2010, ApJS, 186, 427
Price J., Phillipps S., Huxor A., Smith R. J., Lucey J. R., 2011, MNRAS, 411, 2558
Rahman M., Pearson L. M., Heien H. C., 2006, Bull. Malaysian Math. Sci. Soc., 29, 11
Renzini A., 2006, ARA&A, 44, 141
Rix H.-W., White S. D. M., 1990, ApJ, 362, 52
Sandage A., Freeman K. C., Stokes N. R., 1970, ApJ, 160, 831
Scott N., Davies R. L., Houghton R. C. W., Cappellari M., Graham A. W., Pimbblet K. A., 2014, MNRAS, 441, 274
van den Bergh S., 1990, ApJ, 348, 57
Vincent R. A., Ryden B. S., 2005, ApJ, 623, 137
Vulcani B. et al., 2011, MNRAS, 413, 921
Weijmans A.-M. et al., 2014, MNRAS, 444, 3340
Whitmore B. C., Gilmore D. M., Jones C., 1993, ApJ, 407, 489
Willett K. W. et al., 2013, MNRAS, 435, 2835

APPENDIX A: MOMENTS ELLIPTICITY

KR05 use the weighted second-order moments of the r'-band surface brightness I to measure the shape of galaxies. Following Bernstein & Jarvis (2002) they use a Gaussian weight function $w(r, c)$ matched to the size and shape of the galaxy being measured (r and c are the rows and columns in the image). If we define

$$\langle f \rangle_w \equiv \frac{\int f(r, c) w(r, c) I(r, c) dr\, dc}{\int w(r, c) I(r, c) dr\, dc}, \tag{A1}$$

then the centre of the galaxy is given by

$$(r_0, c_0) \equiv (\langle r \rangle_w, \langle c \rangle_w) \tag{A2}$$

and the (central) second moments are defined as

$$M_{rr} \equiv \langle (r - r_0)^2 \rangle_w$$
$$M_{rc} \equiv \langle (r - r_0)(c - c_0) \rangle_w$$
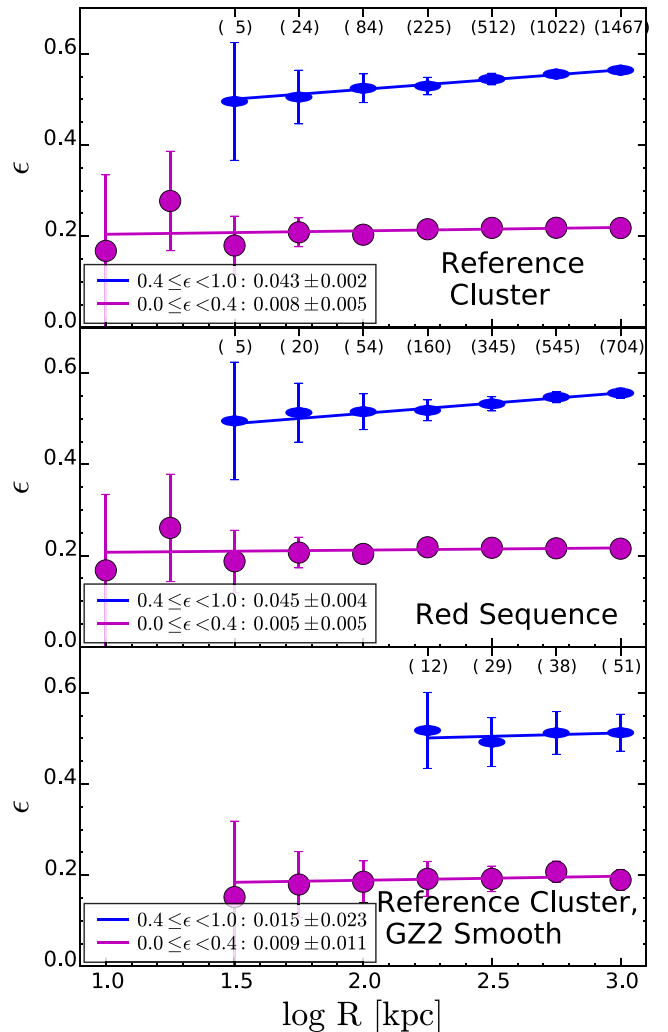$$M_{cc} \equiv \langle (c - c_0)^2 \rangle_w. \tag{A3}$$

Figure A1. Same as Fig. 6, but using the projected moments ellipticity $\epsilon_{\text{moments}}$. The method of moments, as implemented in SDSS, gives smaller values than ϵ_{model}. The sample of flat galaxies ($\epsilon \geq 0.4$) is therefore smaller, and it is impossible to assess any trend from the GZ2 cross-correlated sample. (A colour version of this figure is available in the online version.)

From these quantities, we can define

$$\tau \equiv M_{cc} + M_{rr} \rightarrow \text{mRrCr}$$

$$e_+ \equiv \frac{M_{cc} - M_{rr}}{\tau} \rightarrow \text{mE1}$$

$$e_\times \equiv \frac{2\,M_{rc}}{\tau} \rightarrow \text{mE2}$$

$$e \equiv \sqrt{e_+^2 + e_\times^2}, \tag{A4}$$

where *mRrCc*, *mE1* and *mE2* are the corresponding entries in the SDSS data base. The axial ratio is given by

$$q \equiv \sqrt{\frac{1-e}{1+e}} \tag{A5}$$

and finally we define the projected ellipticity ϵ as

$$\epsilon \equiv 1 - q. \tag{A6}$$

In order to correct for the effect of the PSF, we follow again Bernstein & Jarvis (2002), which use the fourth-order moment as well as the moments of the PSF itself (these data are included in the SDSS data base).

When we use $\epsilon \equiv \epsilon_{\text{moments}}$, the ϵ–R relation is still observed (Fig. A1). However, given that generally we have $\epsilon_{\text{moments}} < \epsilon_{\text{model}}$ (Section 2.1), we have fewer flat galaxies ($\epsilon_{\text{moments}} \geq 0.4$). Therefore, we cannot use $\epsilon_{\text{moments}}$ to constrain the ϵ–R relation of smooth, flat galaxies (bottom panel in Fig. A1).

This paper has been typeset from a TeX/LaTeX file prepared by the author.